










Molecular-rotation-induced splitting of the binary ridge in the velocity map of sub-eV H^+ ions ejected from H_2 molecules by ion impact

Z. Juhász ^{1,*}, S. T. S. Kovács ¹, V. Vizcaino ², P. Herczku ¹, S. Demes ¹, R. Rácz,¹ B. Sulik ¹, S. Biri ¹, N. Sens,²
D. V. Mifsud ^{3,1} and J.-Y. Chesnel ²

¹*Institute for Nuclear Research (Atomki), Debrecen H-4026, Hungary*

²*Centre de Recherche sur les Ions, les Matériaux, et la Photonique (CIMAP), UMR 6252 CEA-CNRS-ENSICAEN-UNICAEN, Normandie Université, 14000 Caen, France*

³*Centre for Astrophysics and Planetary Science, School of Physical Sciences, University of Kent, Canterbury CT2 7NH, United Kingdom*



(Received 25 April 2022; accepted 7 December 2022; published 19 January 2023)

In studies of ion-induced molecular fragmentation, the challenging measurement of the velocity distribution of fragments emitted below 1-eV kinetic energy is rarely achieved, although most fragments have an energy below this value. Here, we study H^+ fragment emission in collisions of 10-keV O^+ ions with H_2 molecules using a field-free time-of-flight technique developed specifically to detect sub-eV fragments. We find that, in the velocity map, the binary ridge due to direct H^+ knockout is split into two parts arising from the rotational motion of the H_2 molecule, and that this split scales with rotational velocity. The velocity distribution of the nuclei in the original molecule is determined and the thermally populated $J = 1$ rotational level is found to be the dominant contributor, although asymmetry in the split indicates projectile-induced rotational transitions between M sublevels. These rotation effects influence fragment emission probabilities, thus carrying important consequences for the radiation-induced hydrogen loss and H_2 dissociation in the atmospheres or exospheres of planets and moons.

DOI: [10.1103/PhysRevA.107.L010801](https://doi.org/10.1103/PhysRevA.107.L010801)

The simplest case of ion-induced molecular fragmentation is that of H_2 . Even in this case, however, diverse processes may occur [1,2]. Following double electron removal, the residual molecule undergoes Coulomb explosion, which results in a quasi-isotropic emission of H^+ at emission energies of ~ 9.5 eV [1,2]. More moderate excitation or single ionization leads to even more intense emission in the sub-eV range [2,3]. Despite its astrophysical relevance as a contributor to exospheric mass loss, this low-energy regime is scarcely studied. Complete energy and angular distributions of emitted fragments are challenging to measure, although their characterization is of great importance since the emission may be anisotropic due to effects of charged particles on fragmentation dynamics. Furthermore, the energy spacing of the first two rotational levels of H_2 is ~ 15 meV, which is large compared to that of other diatomic molecules. As such, the kinetic energy stored in the rotational degree of freedom of H_2 may also influence the fragment distribution in the sub-eV range.

The rotational excitation of molecules colliding with atoms and other molecules was previously studied using the velocity map imaging (VMI) technique for collision velocities of a few hundred meters per second [4–7]. In the resultant two-dimensional velocity maps, the scattered neutral partners (after having been state-selectively ionized by a laser pulse and accelerated by the VMI electric field) show a structured

distribution due to the quantized energy defects arising from transitions between rotational energy levels.

Sub-eV fragments from N_2 generated by electron impact were studied using a time-delayed spectroscopic technique [8]. In another study, fragments down to 0.5 eV emission energy near the 90° emission angle were investigated in the dissociative charge exchange and ionization of O_2 by H^+ and O^+ ions of 10 to 100 keV kinetic energy using a time-of-flight (TOF) technique [9]. Such work is applicable to astrophysics: the escape velocity of the Jovian moon Europa corresponds to ~ 0.3 -eV fragment energy, meaning that dissociation products may leave the lunar exosphere only if their energy exceeds this value due to charge exchange collisions with magnetospheric ions. For H_2 , thermal escape dominates, but charge exchange and knockout processes are also relevant [10]. However, cross sections in the sub-eV emission energy range are often lacking for exospheric models.

The near-complete energy and angular distributions of H^+ fragments were studied using electrostatic spectrometry [1,11,12]. Unfortunately, this technique has a practical low-energy limit of about 2 eV. Several studies have also considered laser-induced fragmentation of H_2 and acquired complete velocity maps using TOF techniques; however, these studies focused on the Coulomb explosion process in the range of a few eV [13,14]. Other groups investigated the angular distribution of the scattered projectile in the H^+ -induced fragmentation of H_2 to demonstrate the projectile's coherence effects [2,15]. Earlier, detailed studies were performed for collisions between O^+ and H_2 , but at energies of several tens of eV and focusing on the reactive

*zjuhasz@atomki.hu

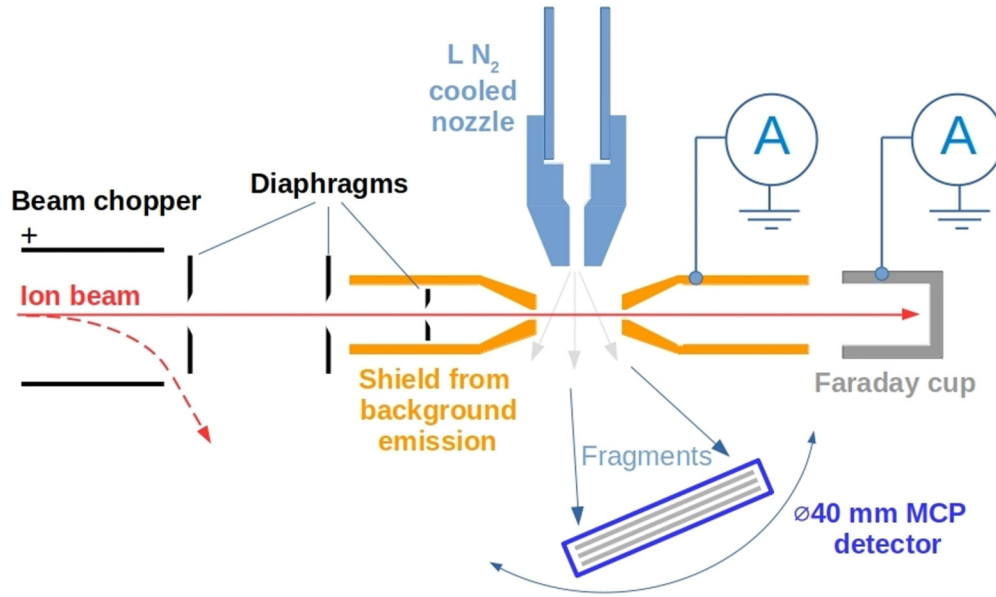


FIG. 1. The field-free TOF experimental setup.

(hydrogen transfer) channel and velocity distributions of the OH^+ product [16,17].

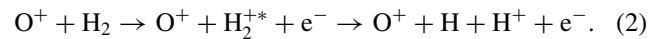
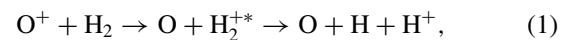
In this Letter, an experimental observation of the effects of the rotational motion of H_2 on the velocity map of positively charged fragments is presented. A field-free TOF technique was used and allowed us to measure accurately the fragment velocity distribution down to 0.1-eV emission energy, thus providing cross sections for collision-induced H^+ emission from H_2 in the sub-eV energy range. The rotational effects, which cause a shift in the velocity map, are observed in the low-energy part of the binary ridge due to the direct knockout of a H^+ fragment by the projectile ion. We show that the present findings are of both fundamental and applied interest, as they give an insight into the nuclear wavefunction of the rotating molecule and may also have astrophysical applications.

The velocity map of the emitted H^+ fragments arising from the impact of H_2 with O^+ ions has been studied over a 0.1- to 20-eV energy range. The reason behind selecting O^+ ions as projectiles is that they are a major constituent of the Jovian magnetosphere and can be easily distinguished from the light H^+ fragments. This Letter focuses on emission energies < 1 eV to demonstrate the effects of molecular rotation. Projectile ions with energies of 10 keV, which correspond to typical stellar wind and Jovian magnetospheric ion velocities [9,18], were provided by an electron cyclotron resonance ion source at Atomki [19]. The ion beam was chopped using the clock signal of the TOF apparatus, and 250-ns ion bunches with 5-kHz repetition frequency were delivered into a vacuum chamber, where they crossed with an effusive gas jet of H_2 supplied by a nozzle cooled to 125 K. The TOF of the emitted H^+ was measured by a position-sensitive microchannel plate detector, which could be set to different observation angles with respect to the beam.

The position and TOF of the detected fragments were used to calculate their velocity vector. The gas jet velocity is estimated to be 1380 m/s, which is comparable to that of

the slowest detected fragments and was therefore subtracted from the calculated fragment velocity vectors. The transversal velocity spread of the jet, estimated to be 140 m/s, induces only a small blurring of the measured velocity distributions. These velocity estimations were based on previous simulations of gas expansion through a nozzle [20]. To ensure that no magnetic or electric fields could change the velocity of the emitted charged fragments, a μ -metal double shield reduced the magnetic field to ~ 1 milligauss at the center of the chamber, and metals with similar contact potentials were used throughout to avoid static electric fields. Moreover, the detector (set to a high surface potential) was shielded electrically by a triple metallic grid arrangement. To minimize the detection of fragmentation products from background gases, narrow metallic tubes were placed around the ion beam with a 3-mm opening at the collision area. The experimental setup is depicted in Fig. 1, and is expounded upon in Ref. [21].

In this study, H^+ fragments may arise from dissociative charge transfer (which is dominant at the present projectile velocity), or dissociative ionization after the formation of H_2^+ :



H^+ emission from the $1s\sigma_g$ ground state occurs mostly at emission energies below 0.1 eV, while emission from the $2s\sigma_g$ and $2p\sigma_u$ excited states of H_2^{+*} occurs over the 4- to 12-eV range [2,3]. The corresponding cross sections integrated over the solid angle and energies as obtained from the velocity maps produced in this work are, respectively, 7 and 1×10^{-16} cm² over these energy ranges, indicating that excitation is not a strong channel in this collision system. However, we note that the cross sections are subject to a systematic

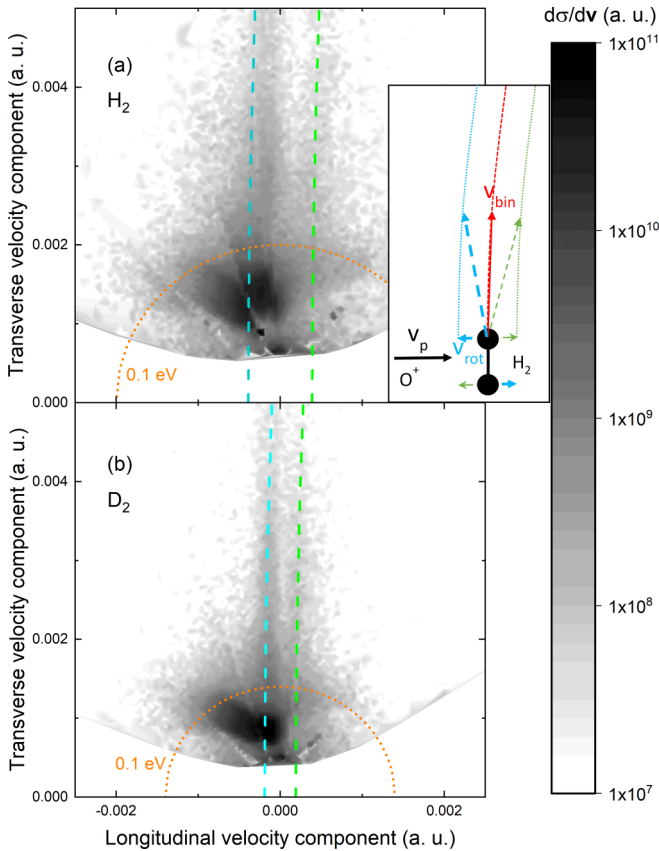


FIG. 2. Velocity distributions of (a) H^+ and (b) D^+ ions, respectively, arising from H_2 or D_2 molecules in collision with 10-keV O^+ ions. The atomic velocity unit is used. The cross section $\frac{d\sigma}{dv}$ for H^+ (or D^+) emission (differential in emission velocity v) is also given in atomic units. The ridges for the direct H^+ (or D^+) binary knockout process are marked by segmented lines. The nozzle was placed 5 mm away from the ion beam axis. Velocities corresponding to a kinetic energy of 0.1 eV are marked by dotted lines for reference. The intense spots below this line at a backward emission angle of $\sim 135^\circ$ are mostly due to dissociative charge transfer processes [Eq. (1)]. The expected isotropic distribution at such low emission velocities is distorted by the spurious field of surface charges. (Inset) The expected binary ridge for a target at rest (red dashed line) and the shifted binary ridges (blue and green dotted lines) caused by molecular rotation. The $\frac{d\sigma}{dv}$ values over the binary ridges are given in tabular form in the Supplemental Material Tables S1 and S2 [22].

uncertainty of at least 15% due to limitations in the accuracy of the pressure gauge. In particular, the cross section for the <0.1 -eV energy range should be regarded with caution, since this range is below the limit of accurate measurement. In this range, the emission appears as being anisotropic [see Fig. 2(a)], while one would expect an isotropic distribution for dissociative charge transfer processes in large-impact parameter collisions. Actually, the low-energy fragment distribution (<0.1 eV) is disturbed by the field of unavoidable surface charges. Moreover, the possible contribution of the H_2^+ molecular ion should be considered: some of the ground-state H_2^+ ions that are produced may remain intact after the collisions, the process of which does not involve kinetic energy release, thus rendering the expected emission energy close to zero.

However, by repeating the experiment and biasing one of the grids placed in front of the detector, the yield of H_2^+ was found to be negligible compared to that of H^+ . The obtained H^+ fragment velocity distribution in the low-velocity range (<0.5 -eV emission energy) in Fig. 2(a).

In the region above the 0.1-eV energy level indicated in Fig. 2, emitted H^+ fragments exhibit an anisotropic distribution as a result of their direct knockout by the projectile. The corresponding tabular-form cross-sectional data are given in the Supplemental Material Table S1 [22]. H^+ fragments produced in this way from a target at rest are expected to be distributed along a binary ridge that appears as an arc in the two-dimensional velocity map, starting at the origin and spreading along the transversal direction. This arc has a radius of

$$v_r = v_p m_O / (m_H + m_O) = 0.139 \text{ a.u.}, \quad (3)$$

where $v_p = 0.148$ a.u. is the projectile velocity and m_H and m_O are the masses of the target H nucleus and O^+ projectile, respectively. This radius is large when compared to the dimensions of Fig. 2. In the velocity map, however, two arcs are visible that are shifted from the origin in the longitudinal direction.

The inset in Fig. 2 provides a graphical explanation of the shifted binary ridges. In collisions involving relatively small impact parameters ($b < 1.4$ a.u.), in which only one target atom is approached, that atom and the projectile jointly determine the collision dynamics. The velocity v_{rot} of the atom in the rotating molecule adds to the velocity v_{bin} gained by binary momentum transfer, the latter being almost transversal. Depending on its sign, the longitudinal component of v_{rot} shifts the binary ridge either backward or forward along the projectile axis. Hence, this component splits the expected ridge for a nonrotating target into two ridges. Conversely, the transversal component of v_{rot} has a negligible influence on the ridge arc, which is nearly a vertical line.

The initial population of the rotational levels of the H_2 gas is determined by the room-temperature Boltzmann distribution. The cooling of the nozzle and the rapid jet expansion cannot change the population [20], which requires several hours to equilibrate. Calculations show that the $J = 1$ rotational level is the most important (66%), and its contribution is thus expected to dominate the H^+ fragment velocity distribution. At the $J = 1$ level, the average H atom velocity v_{rot} is 3.9×10^{-4} a.u., based on the classical formula for angular momentum,

$$J = m_H r_0 v_{\text{rot}}, \quad (4)$$

where $r_0 = 1.4$ a.u. is the internuclear distance in H_2 at equilibrium. Nearly the same shift sizes are observed in both the positive and negative directions, which may stem from the two rotational directions or from the emission of two counter-moving atoms at $J = 1$. To confirm the rotational origin of the binary ridge split, the experiment was repeated using a D_2 target [Fig. 2(b)]. Since D has twice the mass of H, the rotational velocity and, by extension, the induced shifts, are expected to be half of those observed for H_2 assuming that the contribution of the $J = 1$ level remains the most dominant. The velocity map depicted in Fig. 2(b) confirms our

expectations (tabular-form data are given in the Supplemental Material Table S2 [22]).

The fragment distribution along the longitudinal velocity axis provides an insight into the rotational wavefunction of the original target molecule in the longitudinal velocity space. In a similar collision process between H_2^+ and He, it was shown that the spatial imaging of the vibrational wavefunction of H_2^+ is possible by Coulomb explosion imaging, where the only limiting factor stems from the Heisenberg uncertainty relations [23]. Although pump-probe laser experiments have been extensively exploited to study rotational wave packets providing spatial information on the molecular axis distribution [24], the imaging of low- J rotational eigenstates remains scarce [25]. In our case, the insight into the velocity space is possible because the original target atom velocity can be traced back from the two-body kinematics of the binary collision, since the effect of the third atomic center is negligible. In Fig. 3, a double-peaked structure is observed in the longitudinal velocity distributions for both H_2 and D_2 , and stems from the ridge split caused by the rotational motion of the molecules. The distance between peaks for D_2 [Fig. 3(b)] is about half of that for H_2 [Fig. 3(a)] due to the factor-of-two difference between the rotational velocities of these targets.

These curves are compared to the velocity distribution of the nuclei in the molecules calculated using the approximate nuclear wavefunction of a rotating molecule in its vibrational ground state:

$$\Psi \approx \exp[-m\omega(r-r_0)^2/2]Y_{JM}(\theta, \varphi), \quad (5)$$

wherein polar coordinates (r, θ, φ) are defined with a polar axis perpendicular to the scattering plane; Y_{JM} is the spherical harmonic function for the $J = 1$ rotational and $M = \pm 1$ angular momentum projection quantum numbers, r_0 is the internuclear distance in H_2 (or D_2) at equilibrium, m is the atomic mass of H (or D), and ω is the molecular vibration angular frequency.

The blue dotted lines in Fig. 3 correspond to the application of a Fourier transformation in the longitudinal direction at each axis parallel to the initial projectile velocity so as to obtain the longitudinal velocity distributions, with results being coherently added. The probability distribution in the velocity space is derived from the square of the absolute value of the results. The resultant peak positions match those obtained when using the classical formula [Eq. (4)] for angular momentum (3.9×10^{-4} and 1.9×10^{-4} a.u. for H_2 and D_2 , respectively), but the experimental peak positions are marginally closer to the origin.

When incoherent superposition was applied (red dashed lines in Fig. 3), the resultant peak positions matched the experimental ones. However, the dip in the origin was not reproduced and, thus, coherent superposition was a better approach in this respect. These observations suggest that the wavefunction imaging by the projectile appears to be in line with a partial coherent superposition. This is also expected from the coherence properties of the ion beam given the slit geometry [2,15]: the transversal coherence length of the projectile at the collision center is in the range of 1 a.u., which is comparable to the size of the nuclear wavefunction.

It should be noted that the absolute intensities of the binary ridges are significantly smaller for D_2 than for H_2 . The total

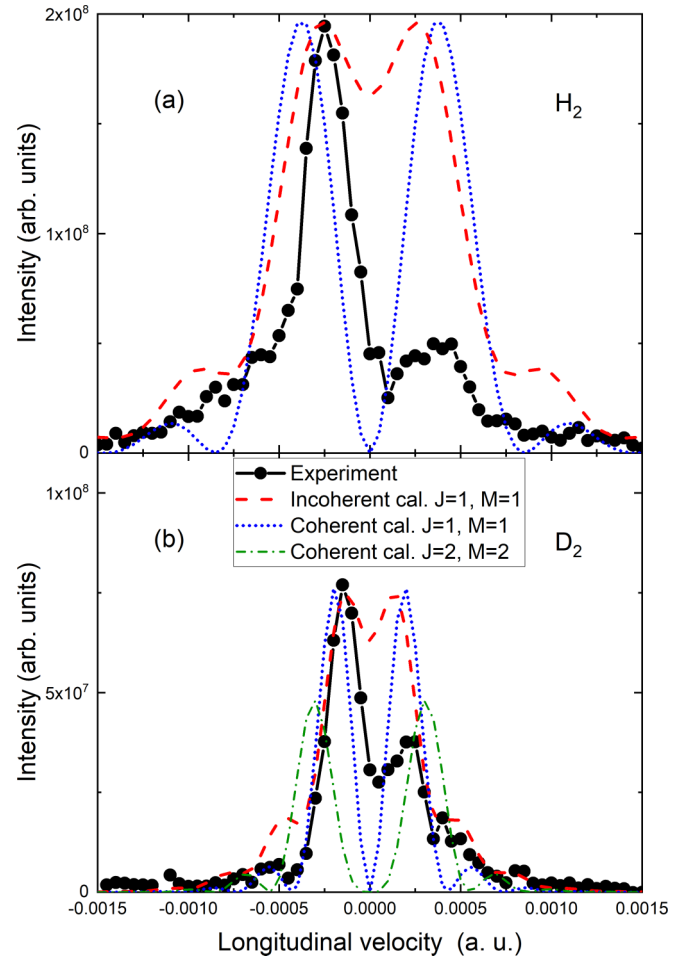


FIG. 3. Measured nuclear velocity distributions in the longitudinal direction (joined circles) with (a) H_2 and (b) D_2 targets. The results are averaged over 0.003 to 0.004 a.u. transversal velocities for good statistics, and v_{bin} was subtracted. The calculated velocity distributions from the nuclear wavefunction for the rotational quantum numbers $J = 1$, $M = \pm 1$ are also shown when coherent superposition (blue dotted line) and incoherent superposition (red dashed line) were applied in the transversal direction. These theoretical curves are normalized to the experiments at the maximum. In (b), the result for the coherent calculation for $J = 2$, $M = \pm 2$ is shown by the green dashed-dotted line with the same normalization as that of the coherent calculation for $J = 1$, $M = \pm 1$, thus permitting the comparison of their intensities.

cross sections for the binary ridges in the energy range 0.1 to 4 eV are 2.5 and $4.9 \times 10^{-16} \text{ cm}^2$, respectively. Similar isotopic effects were observed in Refs. [26,27]. For our total cross section for dissociation via excited molecular ions over the 4- to 12-eV range, the value of $0.45 \times 10^{-16} \text{ cm}^2$ for D_2 may be compared to that of $1 \times 10^{-16} \text{ cm}^2$ for H_2 . Kusakabe *et al.* [26] attributed this difference to the more compact vibrational states of the D_2 isotopologue and the corresponding smaller Franck–Condon factors. Interestingly, in the low-energy region (< 0.1 eV), the opposite trend is observed in our results: $20 \times 10^{-16} \text{ cm}^2$ for the D_2 isotopologue compared to $7 \times 10^{-16} \text{ cm}^2$ for H_2 . However, these values should be regarded with caution due to uncertainties induced by possible instrumental surface charge effects.

A striking difference between the experiment and theory is the strong experimental asymmetry compared to the theoretical symmetry of the distributions. This may be explained by collision-induced rotational excitation of the molecules. The attractive force between the incoming O^+ ion and the approached H atom exerts a torque on the molecule, causing the H atom to, more likely, move backward rather than forward. This is reflected in the more intense peak on the negative side of Fig. 3(a). For D_2 , the asymmetry is smaller [Fig. 3(b)] as a result of its larger moment of inertia.

For H_2 at 300 K, the population of the $J = 0$ level (13%) is small compared to the $J = 1$ level (66%). This explains why a significant contribution from $J = 0$, which would lead to a peak at zero velocity in Fig. 3(a), is not observed. However, precollisional rotational excitations induced by the torque exerted by the projectile on the molecule can affect the population of the observed rotational levels. Although transitions between odd and even rotational levels in H_2 are nuclear-spin forbidden, transitions between states characterized by different $M = -1, 0, 1$ angular momentum projection quantum numbers are likely given that there is no energy change involved during transition. The excitations result in a nonequilibrium M distribution, which is dependent on the impact parameter of the collision with respect to the molecular center. This is the quantum mechanical analog of the explanation of the observed asymmetric velocity distributions in Fig. 3, since the resulting M distribution is such that the projectile will collide with the countermoving atom in the molecule with a higher probability.

Since the energy spacing of the D_2 rotational levels is smaller than that of H_2 , the equilibrium population of the first few rotational levels of D_2 at room temperature is more evenly distributed. From $J = 0$ to $J = 4$, they are respectively 19%, 21%, 39%, 11%, and 9%, according to Boltzmann population calculations. It is perhaps intuitive to expect that the contribution from the $J = 2$ level is dominant in the longitudinal velocity distribution in Fig. 3(b), but our results demonstrate the dominance of the $J = 1$ level, as in the case of H_2 . This may be explained by comparing the intensities resulting from the coherent calculation for the different rotational states shown in Fig. 3(b): higher rotational levels having more nodes possess more evenly balanced positive and negative parts, which results in lower relative contributions due to destructive interference. As shown in Fig. 3(b), the resultant intensity for the $J = 1, M = \pm 1$ rotational state is twice that of the $J = 2, M = \pm 2$ state. Conversely, when the wavefunction is antisymmetric to the polar axis, as in the case of the $J = 2, M = \pm 1$ and the $J = 1, M = 0$ states, interference is fully destructive and results in no intensity being observed from these states. Despite this, however, the contribution of high- J states is indeed noticeable for D_2 [Fig. 3(b)] from the larger peak width compared to that obtained by coherent calculation. This apparent broadening is the result of the merging of peaks for multiple J values.

Higher charge state projectiles presumably initiate more efficient rotational excitations since the interaction with the

molecule is stronger. To demonstrate this, experiments were also performed with 20-keV O^{2+} projectiles, the results of which are described in Ref. [21]. Briefly, the main finding is that the appearance of the higher level rotational excitations suggests that transitions between different J states are open for the doubly charged projectile, in contrast to the singly charged projectile. The observed $J = 3$ state is mainly due to the projectile-induced transition from the thermally populated $J = 1$ state, while the $J = 2$ state is sourced from the $J = 0 \rightarrow 2$ transition.

In conclusion, we have measured the velocity distribution of sub-eV fragments from H_2 (D_2) arising from collisions with 10-keV O^+ ions. The binary ridge of the knocked-out H^+ (D^+) ions is found to be split into two parts. By comparing the isotopologues, we have shown that this phenomenon results from molecular rotational motion, and the split binary ridge provides an insight into the nuclear wavefunction of the rotating molecule in the momentum (velocity) space. We have observed strong isotopic effects in terms of cross sections. Asymmetry in the left- and right-shifted binary ridges indicates rotational transitions prior to the dissociation of the molecule. Using singly charged projectile ions, these transitions are between states associated with different M angular momentum projection quantum numbers, while when using doubly charged projectiles, transitions between different J rotational states may occur.

The molecular rotation effects described in this Letter may greatly influence fragment emission processes, as evidenced by our results. This may have important consequences in astrophysics, where rates of H_2 destruction by stellar winds or magnetospheric ions may significantly differ in the atmospheres of warm planets compared to the rotationally relaxed cooler atmospheres (or exospheres) of comets and moons. This may be particularly important on Earth, where reactive collisions between O^+ ions and H_2 play an important role in atmospheric chemistry, since small changes in the concentration of H_2 may result in large perturbations in the ionosphere [28]. Small rotational effects have already been documented in the production of OH^+ [29]. The present study indicates that the influence of rotational motion on the fragmentation process is important to consider.

This work was supported by the Hungarian Scientific Research Fund of the National Research, Development and Innovation Office financed under the K18 funding scheme through Project No. K128621, and by the Centre National de la Recherche Scientifique (CNRS, France) through International Emerging Action (IEA-PICS-CNRS No. 7739 & Project NKM-115/2017). This article is based upon work from COST Action CA18212–Molecular Dynamics in the GAS phase (MD-GAS), supported by COST (European Cooperation in Science and Technology). Z.J. is grateful for the support of the Hungarian Academy of Sciences through the János Bolyai Research Scholarship. D.V.M. is the grateful recipient of a University of Kent Vice-Chancellor's Research Scholarship.

- [1] P. Sobocinski, J. Rangama, G. Laurent, L. Adoui, A. Cassimi, J.-Y. Chesnel, A. Dubois, D. Hennecart, X. Husson, and F. Frémont, *J. Phys. B: At. Mol. Opt. Phys.* **35**, 1353 (2002).
- [2] B. R. Lamichhane, A. Hasan, T. Arthanayaka, M. Dhital, K. Koirala, T. Voss, R. A. Lomsadze, and M. Schulz, *Phys. Rev. A* **96**, 042708 (2017).
- [3] M. Waitz, R. Y. Bello, D. Metz, J. Lower, F. Trinter, C. Schober, M. Keiling, U. Lenz, M. Pitzer, K. Mertens, M. Martins, J. Viehhaus, S. Klumpp, T. Weber, L. Ph. H. Schmidt, J. B. Williams, M. S. Schöffler, V. V. Serov, A. S. Kheifets, L. Argenti *et al.*, *Nat. Commun.* **8**, 2266 (2017).
- [4] G. Sarma, S. Marinakis, J. J. ter Meulen, D. H. Parker, and K. G. McKendrick, *Nat. Chem.* **4**, 985 (2012).
- [5] J. Onvlee, S. N. Vogels, A. von Zastrow, D. H. Parker, and S. Y. T. van de Meerakker, *Phys. Chem. Chem. Phys.* **16**, 15768 (2014).
- [6] Z. Gao, T. Karman, S. N. Vogels, M. Besemer, A. van der Avoird, G. C. Groenenboom, and S. Y. T. van de Meerakker, *Nat. Chem.* **10**, 469 (2018).
- [7] Z. Gao, J. Loreau, A. van der Avoird, and S. Y. T. van de Meerakker, *Phys. Chem. Chem. Phys.* **21**, 14033 (2019).
- [8] N. Ferreira, L. Sigaud, V. L. B. de Jesus, A. B. Rocha, L. H. Coutinho, and E. C. Montenegro, *Phys. Rev. A* **86**, 012702 (2012).
- [9] H. Luna, C. McGrath, M. B. Shah, R. E. Johnson, M. Liu, C. J. Latimer, and E. C. Montenegro, *Astrophys. J.* **628**, 1086 (2005).
- [10] R. E. Johnson, M. H. Burger, T. A. Cassidy, F. Leblanc, M. Marconi, W. H. Smyth, and R. Dotson, Composition and detection of Europa's sputter-induced atmosphere, in *Europa*, edited by R. T. Pappalardo, W. B. McKinnon, and K. K. Khurana (University of Arizona Press, Tucson, 2009), pp. 507–528.
- [11] F. Frémont, C. Bedouet, M. Taxisien, L. Adoui, A. Cassimi, A. Dubois, J.-Y. Chesnel, and X. Husson, *J. Phys. B: At. Mol. Opt. Phys.* **33**, L249 (2000).
- [12] Z. Juhász, B. Sulik, E. Lattouf, E. Bene, B. A. Huber, P. Herczku, S. T. S. Kovács, A. Méry, J.-C. Pouilly, J. Rangama, J. A. Tanis, V. Vizcaino, and J.-Y. Chesnel, *Phys. Rev. A* **100**, 032713 (2019).
- [13] A. S. Alnaser, X. M. Tong, T. Osipov, S. Voss, C. M. Maharjan, P. Ranitovic, B. Ulrich, B. Shan, Z. Chang, C. D. Lin, and C. L. Cocke, *Phys. Rev. Lett.* **93**, 183202 (2004).
- [14] B. Manschwetus, T. Nubbemeyer, K. Gorling, G. Steinmeyer, U. Eichmann, H. Rottke, and W. Sandner, *Phys. Rev. Lett.* **102**, 113002 (2009).
- [15] B. R. Lamichhane, T. Arthanayaka, J. Remolina, A. Hasan, M. F. Ciappina, F. Navarrete, R. O. Barrachina, R. A. Lomsadze, and M. Schulz, *Phys. Rev. Lett.* **119**, 083402 (2017).
- [16] K. T. Gillen, B. H. Mahan, and J. S. Winn, *J. Chem. Phys.* **58**, 5373 (1973).
- [17] K. T. Gillen, B. H. Mahan, and J. S. Winn, *J. Chem. Phys.* **59**, 6380 (1973).
- [18] S. J. Bolton, F. Bagenal, M. Blanc, T. Cassidy, E. Chané, C. Jackman, X. Jia, A. Kotova, N. Krupp, A. Milillo, C. Plainaki, H. T. Smith, and H. Waite, *Space Sci. Rev.* **192**, 209 (2015).
- [19] S. Biri, I. K. Vajda, P. Hajdu, R. Rácz, A. Csík, Z. Kormány, Z. Perduk, F. Kocsis, and I. Rajta, *Eur. Phys. J. Plus* **136**, 247 (2021).
- [20] A. Naß and E. Steffens, *Nucl. Instr. Meth. Phys. Res. A* **598**, 653 (2009).
- [21] Z. Juhász, S. T. S. Kovács, V. Vizcaino, P. Herczku, S. Demes, R. Rácz, B. Sulik, S. Biri, N. Sens, D.V. Mifsud, and J.-Y. Chesnel (unpublished).
- [22] See Supplemental Material at <http://link.aps.org/supplemental/10.1103/PhysRevA.107.L010801> for the measured double-differential $H^+(D^+)$ fragment emission cross sections.
- [23] L. Ph. H. Schmidt, T. Jahnke, A. Czasch, M. Schöffler, H. Schmidt-Böcking, and R. Dörner, *Phys. Rev. Lett.* **108**, 073202 (2012).
- [24] K. Mizuse, N. Chizuwa, D. Ikeda, T. Imajo, and Y. Ohshima, *Phys. Chem. Chem. Phys.* **20**, 3303 (2018).
- [25] Y. Mi, P. Peng, N. Camus, X. Sun, P. Fross, D. Martinez, Z. Dube, P. B. Corkum, D. M. Villeneuve, A. Staudte, R. Moshhammer, and T. Pfeifer, *Phys. Rev. Lett.* **125**, 173201 (2020).
- [26] T. Kusakabe, L. Pichl, R. J. Buenker, M. Kimura, and H. Tawara, *Phys. Rev. A* **70**, 052710 (2004).
- [27] S. Rai, K. I. Bijlsma, I. Rabadán, L. Méndez, P. A. J. Wolff, M. Salverda, O. O. Versolato, and R. Hoekstra, *Phys. Rev. A* **106**, 012804 (2022).
- [28] M. Yasar and M. Canyılmaz, *Therm. Sci.* **22**, S47 (2018).
- [29] X. Li, Y.-L. Huang, G. D. Flesch, and C. Y. Ng, *J. Chem. Phys.* **106**, 564 (1997).